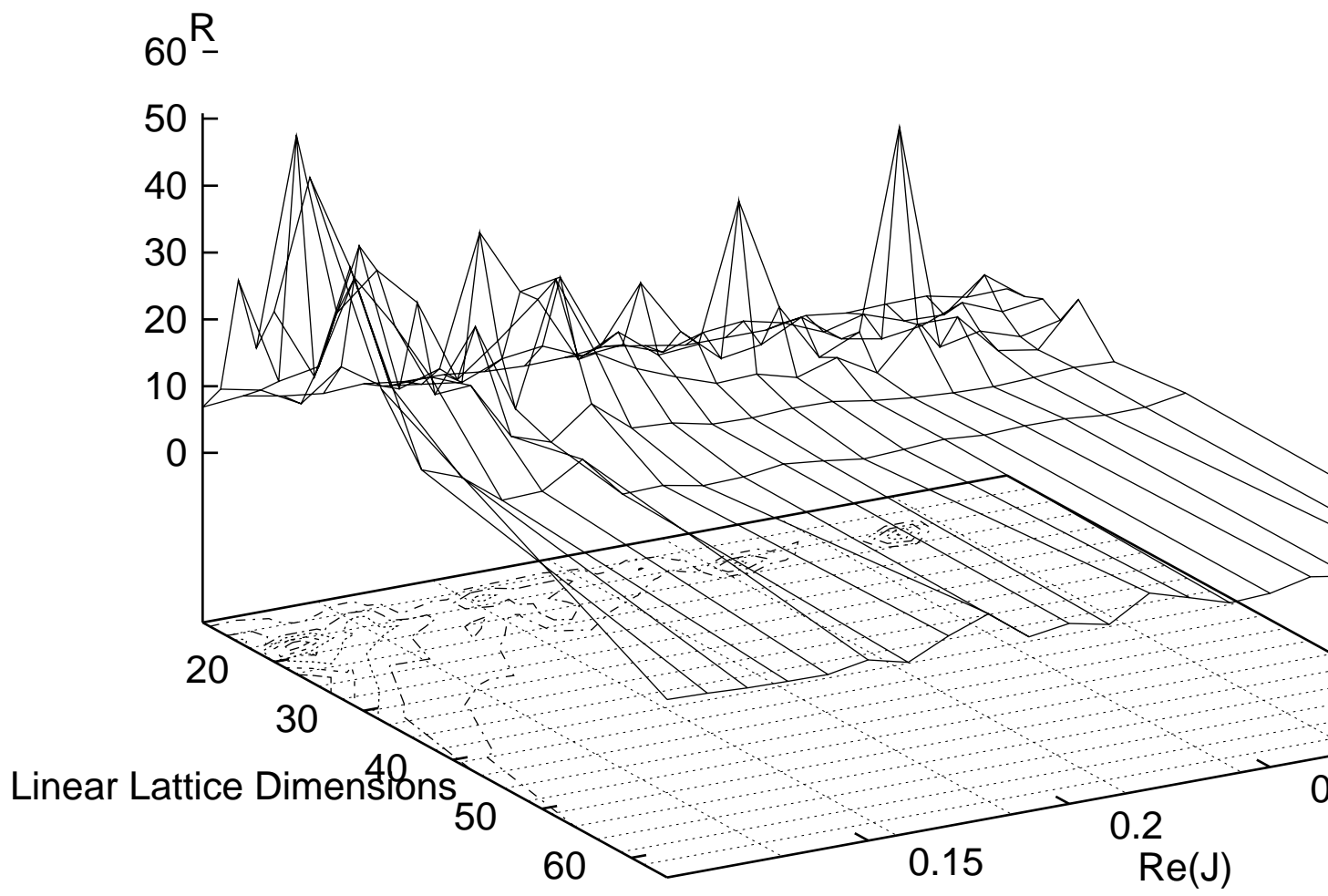
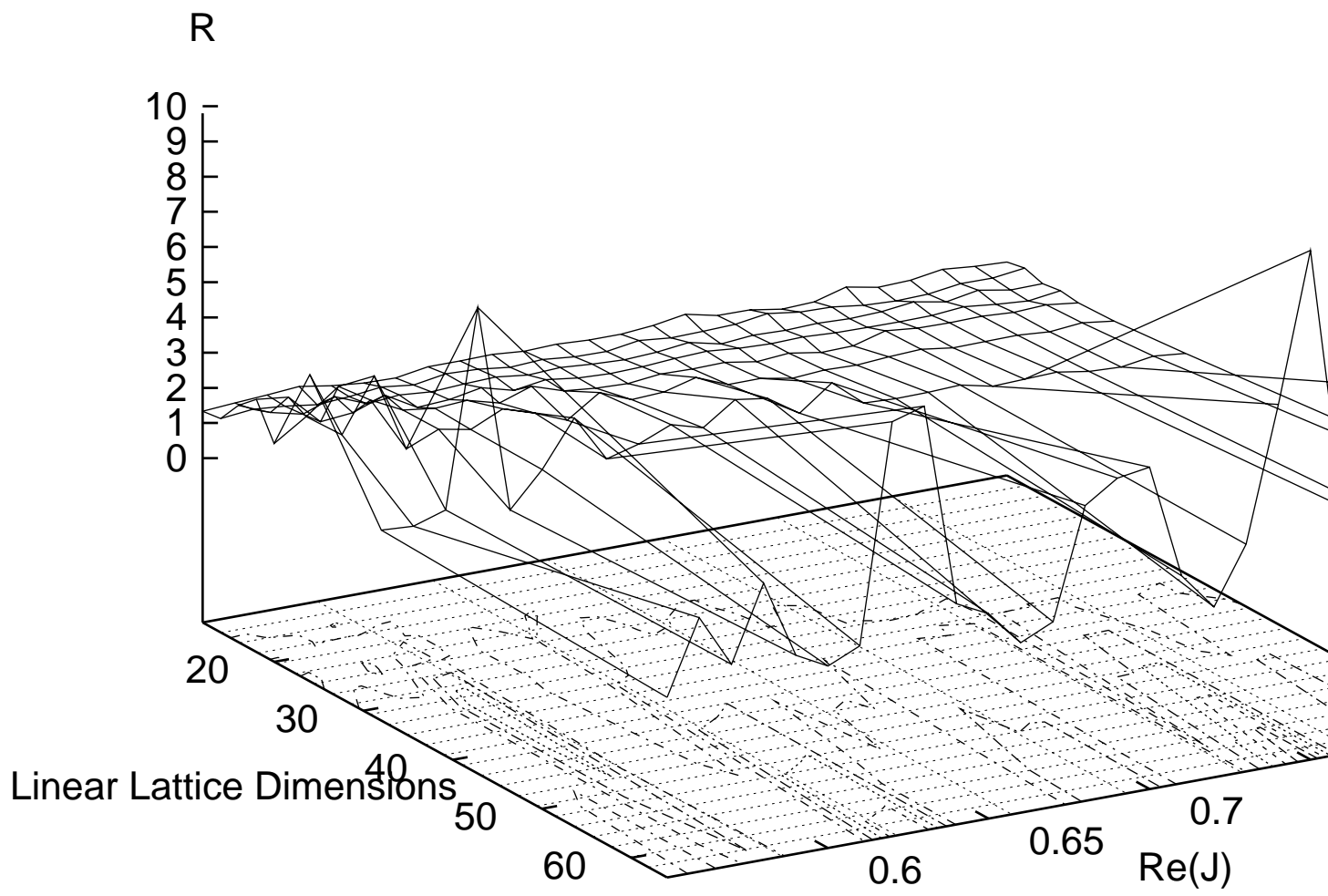


ratio of proporti



ratio of proporti



Simulations with Complex Measure

J F Markham^a and T D Kieu^{a,b}

^aSchool of Physics, University of Melbourne, Parkville 3052, Australia

^bDepartment of Physics, Columbia University, New York, NY 10027, USA

Abstract

A method is proposed to handle the sign problem in the simulation of systems having indefinite or complex-valued measures. In general, this new approach, which is based on renormalisation blocking, is shown to yield statistical errors smaller than the crude Monte Carlo method using absolute values of the original measures. The improved method is applied to the 2D Ising model with temperature generalised to take on complex values. It is also adapted to implement Monte Carlo Renormalisation Group calculations of the magnetic and thermal critical exponents.

1 The Monte Carlo sign problem

In order to evaluate a multi-dimensional integral

$$I \equiv \int f dV \quad (1)$$

using Monte Carlo (MC) one can sample the points in the integration domain with a non-uniform distribution, p , which reflects the contribution from the measure f at each point, as in the *importance sampling* [1]. This sampling gives the following estimate for the integral:

$$I \approx \left\langle \frac{f}{p} \right\rangle \pm \sqrt{\frac{S}{N}}, \quad (2)$$

where N is the number of points sampled, $p \geq 0$ and is normalised

$$\begin{aligned} \int p dV &= 1, \\ \langle f/p \rangle &\equiv \frac{1}{N} \sum_{i=1}^N f(x_i)/p(x_i). \end{aligned}$$

and

$$\begin{aligned} S &\equiv \int \left| \frac{f}{p} - I \right|^2 p dV, \\ &\approx \left\langle \frac{f^2}{p^2} \right\rangle - \left\langle \frac{f}{p} \right\rangle^2. \end{aligned} \quad (3)$$

The best choice of p is the one that minimises the standard deviation squared S . This can be found by variational method leading to the *crude* average-sign MC weight [2]

$$p_{\text{crude}} = \frac{|f|}{\int |f| dV}, \quad (4)$$

giving the optimal

$$S_{\text{crude}} = \left(\int |f| dV \right)^2 - \left| \left(\int f dV \right) \right|^2. \quad (5)$$

Applying to physical systems, MC method can be used to evaluate the expectation value of some measurable quantity Θ

$$\begin{aligned}\langle\Theta\rangle &= \frac{\sum_{\{s\}} \Theta e^{-H}}{\sum_{\{s\}} e^{-H}}, \\ Z &\equiv \sum_{\{s\}} e^{-H},\end{aligned}\tag{6}$$

where s denotes the dynamical variables and H is the hamiltonian of an equilibrium statistical system or the action of some Euclidean quantum field theory.

Since an estimate of the denominator of (6) is independent of a particular measurable and is needed in calculating all observables, it is to this that we apply the MC method. The integral (1) now assumes the form of the partition function Z , upon which the crude weight (4) takes on the explicit form

$$p_{\text{crude}} \rightarrow |e^{-H}| / \sum_{\{s\}} |e^{-H}|.\tag{7}$$

The Boltzmann weight e^{-H} can in general be real but non-definite, or even be complex-valued, in which case it is possible to generalise the absolute values of real numbers in the above expressions to those of complex numbers. And the error bars now can be visualised as the *error radius* in the complex plane of a circle centred at the complex-valued central MC estimate. The variational derivation still goes through as with real numbers.

We then have in the MC approximation

$$\langle\Theta\rangle \approx \frac{\sum_{\text{MCconfigurations}} \Theta \left(e^{-H} / |e^{-H}| \right)}{\sum_{\text{MCconfigurations}} \left(e^{-H} / |e^{-H}| \right)} \equiv \frac{\langle\langle\Theta\rangle\rangle_{\text{crude}}}{\langle\langle\text{sign}\rangle\rangle_{\text{crude}}}.\tag{8}$$

In the above $\langle\langle\text{sign}\rangle\rangle$ also denotes the average, with respect to a given MC weight, of the phase when e^{-H} is complex.

The *sign problem* [3] arises when $|\langle\langle\text{sign}\rangle\rangle|$ is vanishingly small: then unless a huge number of configurations are MC sampled, the large statistical fluctuations of (8), because of the small denominator, render the measurement meaningless.

Unfortunately, many interesting and important physical problems suffer the sign problem like the real-time path integrals of quantum mechanics and quantum field theory, lattice QCD at finite temperature and non-zero chemical potential, lattice chiral gauge theory, quantum statistical system with fermions . . . None of the existing proposals is quite satisfactory: complex Langevin simulations [4] cannot be shown to converge to the desired distribution and often fail to do so; others [5] are either restricted to too small a lattice, too complicated, or not general enough or rather speculative.

In the next section we present another improved method, which is then applied to the Ising model in two dimensions and the results will be compared with the crude MC of this section, as well as with series-expansion data.

2 The improved method

One way of smoothing out the sign problem is to do part of the integral analytically, and the remainder using MC [6]. The analytical summation is not just directly over a subset of the dynamical variables; in general it can be a renormalisation group (RG) blocking where coarse-grained variables are introduced. We will show below that this does yield certain improvement over the crude MC in general.

Let $P\{V', V\}$ be the normalised RG weight relating the original variables V to the blocked variables V' [7],

$$P\{V', V\} \geq 0,$$

$$\int P\{V', V\}dV' = 1.$$

Inserting this unity resolution into the integral (1)

$$\begin{aligned} I &= \int dV \int dV' P\{V', V\}f, \\ &\equiv \int dV' g(V'), \end{aligned} \tag{9}$$

and assuming that the blocking can be done exactly or approximated to a good degree such that we then obtain g as a function of blocked variables in closed form. An example of the RG blocking which we will employ in the next section for the Ising model is the sum over spins on odd sites of the lattice, leaving behind a measure g in terms of the other half of the spins on even sites. Thus, an MC estimator is only needed for the remaining integration over V' in (9). As with the crude method of the last section, variational minimisation for S of (3), with g in place of f , leads to the *improved* MC

$$p_{\text{improved}} = \frac{|g|}{\int |g|dV'}. \tag{10}$$

This one-step exact RG blocking already improves over the crude average-sign method of the last section. Firstly, the improved weight sampling yields in (8) a denominator of magnitude not less than that sampled by the crude weight:

$$\begin{aligned} \left| \langle \langle \text{sign} \rangle \rangle_{\text{improved}} \right| &\equiv \frac{Z}{\int |g|dV'}, \\ &= \frac{Z}{\int \left| \int P\{V', V\}f dV \right| dV'}, \\ &\geq \frac{Z}{\int |f|dV}, \\ &\equiv \left| \langle \langle \text{sign} \rangle \rangle_{\text{crude}} \right|, \end{aligned} \tag{11}$$

where we have used the definitions of the sampling weights in the second equality, g in (9). The inequality is the triangle inequality from the properties

of P . In other words, from their definitions, $\langle\langle\text{sign}\rangle\rangle_{\text{improved}}$ is proportional to $\langle\langle\text{sign}\rangle\rangle_{\text{crude}}$, with the proportionality constant is some function of temperature and external fields. Both of them vanish when the partition function does; away from this point, however, the improved method is no worse than the crude one.

Secondly, it is also not difficult to see that the statistical fluctuations associated with improved MC is not more than that of the crude MC,

$$\begin{aligned}
S_{\text{improved}} - S_{\text{crude}} &= \int \left| \frac{g^2}{p_{\text{improved}}} \right| dV' - \int \left| \frac{f^2}{p_{\text{crude}}} \right| dV, \\
&= \left(\int |g| dV' \right)^2 - \left(\int |f| dV \right)^2, \\
&= \left(\int \left| \int P\{V', V\} f dV \right| dV' \right)^2 - \left(\int |f| dV \right)^2, \\
&\leq 0,
\end{aligned} \tag{12}$$

where we have used the definitions of the sampling weights in the second equality, definition of g (9) in the third. The last inequality is the triangle inequality from the properties of P .

Thus the RG blocking always reduces, sometimes significantly, the statistical fluctuations of an observable measurement by reducing the magnitude of

$$\frac{\sqrt{S}}{|\langle\langle\text{sign}\rangle\rangle|}.$$

Note that the special case of equality in (11,12) occurs *iff* there was no sign problem to begin with. How much improvement one can get out of the new MC weight, i.e. how large are the above inequalities, depends on the details of the RG blocking and on the original measure f .

3 Application to the 2D Ising model

The Hamiltonian for the Ising model on a square lattice is

$$H = -j \sum_{\langle nn' \rangle} s_n s_{n'} - h \sum_n s_n. \quad (13)$$

Here we allow j and h to take on complex values in general. The sum over $\{s\}$ in the partition function is a sum over all possible values of the spins $s_n = \{+1, -1\}$ at site n . The sum over $\langle n'n \rangle$ is a sum over all nearest neighbours on the lattice. For the finite lattice, periodic boundary conditions are used.

The phase boundaries for the complex temperature 2D Ising model with $h = 0$ are found by [8]

$$\begin{aligned} \operatorname{Re}(u) &= 1 + 2^{\frac{3}{2}} \cos \omega + 2 \cos 2\omega \\ \operatorname{Im}(u) &= 2^{\frac{3}{2}} \sin \omega + 2 \sin 2\omega \end{aligned} \quad (14)$$

where ω is taken over the range $0 \leq \omega \leq 2\pi$, and

$$u = e^{-4j}. \quad (15)$$

In the u plane, this is a limaçon, which transforms to the j plane as shown in Fig. 1.

Figure 1: Phase diagram in the complex j plane, $h = 0$.

FM=ferromagnetic, PM=paramagnetic, AFM=antiferromagnetic.

As $e^{-H}/|e^{-H}|$ takes values on the unit circle, the crude MC estimator for the denominator of (8) might be vanishingly small, but its standard variance S is of order unity, leading to the sign problem.

For the improved method, we adopt a simple RG blocking over the odd sites, labeled \circ . That is, the analytic summation is done over the configuration space spanned by the \circ sites; while MC is used to evaluate the sum

over the remaining lattice of the \bullet sites. The following diagram shows the two sublattices, and how the \bullet sites are to be labelled relative to the \circ sites, for the site labelled x .

Figure 2: Relative spin positions on a partitioned lattice.

In general, with finite-range interactions between the spins, one can always subdivide the lattice into sublattices, on each of which the spins are independent and thus the partial sum over these spins could be carried out exactly.

Summing over the spins s_{\circ} ,

$$Z = \sum_{\{s_{\bullet}\}} e^{h \sum_{\bullet \text{ sites}} s_{\bullet}} \prod_{\circ \text{ sites}} 2 \cosh [j s_{\bullet}^+ + h] \quad (16)$$

where $s_{\bullet}^+ \equiv s_{\bullet}^{\uparrow} + s_{\bullet}^{\rightarrow} + s_{\bullet}^{\downarrow} + s_{\bullet}^{\leftarrow}$. The improved MC weight is then the absolute value of the summand on the right hand side of the last expression for Z .

The quantities to be measured are magnetisation, M , and susceptibility, χ . These can be expressed in terms of the first and second derivatives of Z respectively, evaluated at $h = 0$. Using the above notation:

$$\frac{\partial Z}{\partial h} = \sum_{\bullet \text{ spins}} \left\{ \left[e^{h \sum_{\bullet \text{ sites}} s_{\bullet}} \prod_{\circ \text{ sites}} 2 \cosh [j s_{\bullet}^+ + h] \right] \left[\sum_{\circ \text{ sites}} (s_{\bullet}^{\uparrow} + \tanh (j s_{\bullet}^+ + h)) \right] \right\}, \quad (17)$$

and

$$\begin{aligned} \frac{\partial^2 Z}{\partial h^2} = & \sum_{\bullet \text{ spins}} \left\{ \left[e^{h \sum_{\bullet \text{ sites}} s_{\bullet}} \prod_{\circ \text{ sites}} 2 \cosh [j s_{\bullet}^+ + h] \right] \times \right. \\ & \left[\left(\sum_{\circ \text{ sites}} (s_{\bullet}^{\uparrow} + \tanh (j s_{\bullet}^+ + h)) \right)^2 + \right. \\ & \left. \left. \sum_{\circ \text{ sites}} \left(\frac{1}{\cosh^2 (j s_{\bullet}^+ + h)} \right) \right] \right\}. \quad (18) \end{aligned}$$

4 Numerical results

In all the simulations, square two-dimensional lattices of various sizes with periodic boundary conditions are used. After the RG blocking, half the spins go, and the original boundary conditions are maintained. The heat-bath algorithm is used to obtain configurations that are distributed with the required weights. One heat bath sweep involves visiting every site in the lattice once.

4.1 Autocorrelation

Two additional benefits arise from the improved method. The first is that the number of sites to be visited is halved. While the expressions to be calculated at the remaining sites turn out to be far more complicated, the use of table look-up means that evaluating them need not be computationally more expensive. The second benefit is that correlation between successive configurations and hence the number of sweeps required to decorrelate data points is reduced. This correlation is quantified in terms of the *normalised relaxation function* $\phi_A(t)$ for some observed quantity A ,

$$\phi_A(t) = \frac{\langle\langle A(0)A(t)\rangle\rangle - \langle\langle A\rangle\rangle^2}{\langle\langle A^2\rangle\rangle - \langle\langle A\rangle\rangle^2} \quad (19)$$

The following graph is typical of the behavior near to criticality and demonstrates the improvement which is possible. The observable used is the real part of the magnetisation versus the number of sweeps. Table 1 shows the data used in generating Fig. 3.

Figure 3: Autocorrelation of the real parts of magnetisation.

Table 1: Data for Figure 3.

Quantity	Value
Lattice Size	32x32
Total Sweeps	5,000,000
Applied Field, h	0 + 0i
Interaction, j	0.435 + 0.1i
Start	Cold
Walk	Heatbath

4.2 Improved estimate of $\langle\langle \text{sign} \rangle\rangle$

As a test of the improved method, it is compared to the crude one along the path OX in Fig. 1.

Figure 4: $|\langle\langle \text{sign} \rangle\rangle|$ vs $Re(j)$, $Im(j) = 0.1$, $h = 0$

Table 2 shows the data used in generating the remainder of the graphs:

- *Thermalising sweeps* is the number of sweeps performed before data is collected.
- *Data points* is the number of configurations used in a measurement.
- *Sweeps between points* is the number of sweeps performed between measurements.

Note the followings from Fig. 4:

- Both methods fail close to the phase boundary around $Re(j) = 0.4$ (actually actually no methods can work where Z vanishes) and so results for this region are not presented. The important thing is that for a given error, the improved method is able to get closer to the phase boundary than the crude one.

Table 2: Data for Figs. 4-7.

Quantity	Value
Lattice Size	20x20
Thermalising Sweeps	1000
Data Points	1000
Sweeps Between Points	100
Applied Field, h	$0 + 0i$
Interaction, j	$\text{Re}(j) + 0.1i$
Start	Cold
Walk	Heatbath

- In agreement with the analytic consideration of section 2, the error bars on $|\langle\langle \text{sign} \rangle\rangle|$ obtained using the improved method are never worse than for the crude one.
- Especially for $0.1 < j < 0.2$, the improved method has lifted $|\langle\langle \text{sign} \rangle\rangle|$ drastically, showing that $Z \neq 0$ but the crude method cannot. This results in a big improvement on the statistical errors of the observables, as we will see in the following sections. The reason that the value of $|\langle\langle \text{sign} \rangle\rangle|$ is increased more at high temperatures is that the summing of opposite spins in $\cosh [js_{\bullet}^+ + h]$ causes a greater reduction in the variance of $e^{-H} / |e^{-H}|$.

The gains are more striking if we plot the ratio of the proportional errors, R where

$$R_{\text{sign}} = \frac{\left(\frac{S_{\text{sign}}}{\langle\langle \text{sign} \rangle\rangle}\right)_{\text{crude}}}{\left(\frac{S_{\text{sign}}}{\langle\langle \text{sign} \rangle\rangle}\right)_{\text{improved}}}. \quad (20)$$

This is an important comparison because the errors on the physical observables, like magnetisation and susceptibility M and χ , depend on the propor-

tional error of $|\langle\langle \text{sign} \rangle\rangle|$.

Figure 5: R_{sign} vs $Re(j)$, $Im(j) = 0.1$, $h = 0$.

4.3 Improved estimate of $\langle \mathbf{M} \rangle$

The equivalent graphs for estimates of $|\langle M \rangle|$ are presented below. For clarity, in Fig. 6, only every second data point is shown. The data agrees with known behaviour of the magnetisation at high and low temperatures.

Figure 6: $|\langle M \rangle|$ vs $Re(j)$ where $Im(j) = 0.1$, $h = 0$.

Figure 7: Ratio of MC error radii of magnetisation.

4.4 Improved estimate of susceptibility χ

The magnitudes of susceptibility for crude and improved MC are shown in Fig. 8. In the region of OX line in the ferromagnetic phase, both methods are comparable and consistent with zero. Fig. 9 depicts the ratio of error radii of the two simulation methods.

Figure 8: $|\langle \chi \rangle|$ vs $Re(j)$ where $Im(j) = 0.1$, $h = 0$.

Figure 9: Ratio of MC error radii of susceptibility.

Comparison with series-expansion data are plotted in Figs. 10 and 11.

Figure 10: Improved $|\langle \chi \rangle|$ vs $Re(j)$. Expansion shown as line.

Figure 11: Improved $\langle \chi \rangle$ vs $Re(j)$. Expansion shown as line.

The discs in Fig. 11 are the circles of statistical errors for simulated results.

4.5 Dependence on lattice size

Fig. 5 is actually a slice from Fig 12 and Fig 13. These show how the improvement in R_{sign} depends on the linear lattice dimensions. Two interesting trends are apparent:

- At low temperature the amount of improvement increase with lattice size.
- At high temperature the amount of improvement decrease with lattice size. We do not attempt to explain this behavior, but note that for high temperatures one would expect R_{sign} to approach some limiting value for large lattice sizes. The reason for this is as follows. For both methods, the quantity $e^{-H} / |e^{-H}|$ is the sum of arg 's over all sites. Hence, by the central limit theorem for large lattices it is normally distributed. Its variance is a function of the spin statistics, which are not size dependent.

Figure 12: R_{sign} vs $Re(j)$ and linear lattice dimension, $0.1 < Re(j) < 0.3$
 $Im(j) = 0.1$, $h = 0$.

Figure 13: R_{sign} vs $Re(j)$ and linear lattice dimension, $0.5 < Re(j) < 0.8$
 $Im(j) = 0.1$, $h = 0$.

4.6 MC renormalisation group

We explore the MCRG with both the standard and improved methods at the critical temperature on the positive, real axis. It is found that the critical exponents of the blocked lattice are the same as those on the original. The values of the critical exponents γ_0 and γ_1 , measured using MCRG are displayed in Table 3. The exact values of $8/15$ and 1 are shown at the top of the table.

The data used in generating Table 3 is shown in Table 4:

- The *bootstrap method* [10] is used to calculate errors on the critical exponents. The number of bootstrap samples used, B , is 500. In theory, the limit

Table 3: Critical exponents.

RG iterations	γ_0 (0.533)		γ_1 (1.00)	
	Crude	Improved	Crude	Improved
1	0.532(1)	0.546(1)	1.13(4)	1.08(4)
2	0.536(2)	0.539(3)	1.12(5)	1.04(4)
3	0.535(4)	0.539(4)	1.20(7)	1.10(5)
4	0.535(8)	0.519(5)	1.05(7)	1.11(6)

of $B \rightarrow \infty$ should be taken. In practice it is found that the distribution changes little for $B > 500$.

- The results from the crude and improved methods agree within error.
- The consistent deviation from the exact value is in agreement with similar simulations [9] and can be explained by truncation of the hamiltonian during MCRG and finite size effects.
- No improvement should be expected (nor is it observed) as there is no sign problem in this case. The purpose of these figures is only to demonstrate that the improved method is adaptable for use in MCRG.

Concluding remarks

We have presented a method towards a partial alleviation of the sign problem; it is the earlier proposal in [6] generalised to include exact RG transformations. The sign problem is lessened because of some partial phase cancellation among the original indefinite or complex-valued measure after an exact RG transformation.

A particular RG blocking is chosen for our illustrative example of the

Table 4: Data for Table 3.

Quantity	Value
Lattice Size	64x64
Data Points	1000
Sweeps Between Points	8000
Applied Field, h	$0.001 + 0i$
Interaction, j	$0.440687 + 0i$
Start	Cold
Walk	Heatbath
RG Blockings	5
Bootstrap Samples	500

2D Ising model with complex-valued measure. And this summation over a sublattice is the natural choice which always exists for short-ranged interactions. But other choices of RG blocking are feasible and how effective they are depends on the physics of the problems.

When the quantity to be averaged is not smooth on the length scale of the crude weight function, there is an additional source of systematic error in the crude, average-sign method. The cancellation in the partial sums may reduce this error by reducing the difference in length scales of the measured quantities and that of the sampling weights.

Acknowledgements

We are indebted to Robert Shrock for discussions and for providing us the series-expansion data of the susceptibility; to Andy Rawlinson for the preparation of some graphs. One of us, TDK, wants to thank Norman Christ and

the Theory Group at Columbia University for their hospitality during his stay. The authors also wish to thank the Australian Research Council and Fulbright Program for financial support.

References

- [1] K. Binder D. W. and Heermann, *Monte Carlo Simulation in Statistical Physics, An Introduction*, second corrected edition (Springer-Verlag, Berlin Heidelberg New York, 1992).
- [2] H. de Raedt and A. Lagendijk, *Phys. Rev. Lett.* **46**, 77 (1981).
- [3] H. de Raedt and A. Lagendijk in [2];
A.P. Vinogradov and V.S. Filinov, *Sov. Phys. Dokl.* **26**, 1044 (1981);
J.E. Hirsch, *Phys. Rev.* **B31**, 4403 (1985);
For a recent review, see W. von der Linden, *Phys. Rep.* **220**, 53 (1992).
- [4] G. Parisi, *Phys. Lett.* **131B**, 393 (1983);
J.R. Klauder and W.P. Petersen, *J. Stat. Phys.* **39**, 53 (1985);
L.L. Salcedo, *Phys. Lett.* **304B**, 125 (1993);
H. Gausterer and S. Lee, unpublished (preprint October, 1992).
- [5] A. Gocksh, *Phys. Lett.* **206B**, 290 (1988);
S.B. Fahy and D.R. Hamann, *Phys. Rev. Lett.* **65**, 3437 (1990); *Phys. Rev.* **B43**, 765 (1991);
M. Suzuki, *Phys. Lett.* **146A**, 319 (1991);
C.H. Mak, *Phys. Rev. Lett.* **68**, 899 (1992);
A. Galli, unpublished (hep-lat/9605026).
- [6] T.D. Kieu and C.J. Griffin, *Phys Rev E* **49**, 3855 (1994).

- [7] K. Huang, *Statistical Mechanics, Second Edition* (John Wiley and Sons, New York, 1987).
- [8] R. Shrock, *Nucl Phys (Proc Supp)* **B47**, 731 (1996);
V. Matveev and R. Shrock, *J Phys* **A28**, 1557 (1995); *Phys Rev* **E53**, 254 (1996).
- [9] R.H. Swendsen, in *Real-Space Renormalisation*, ed. T.W. Burkhardt and J.M.J. van Leeuwen (Springer-Verlag, Berlin-Heidelberg-New York, 1982).
- [10] B. Efron and R.J. Tibshirani, *An Introduction to the Bootstrap* (Chapman and Hall, New York, 1993).

Table Captions

Table 1: Data for Figure 2.

Table 2: Data for Figs. 4-7.

Table 3: Critical exponents.

Table 4: Data for Table 3.

Figure Captions

Figure 1: Phase diagram in the complex j plane, $h = 0$. FM=ferromagnetic, PM=paramagnetic, AFM=antiferromagnetic.

Figure 2: Relative spin positions on a partitioned lattice.

Figure 3: Autocorrelation of the real parts of magnetisation.

Figure 4: $|\langle\langle \text{sign} \rangle\rangle|$ vs $Re(j)$, $Im(j) = 0.1$, $h = 0$

Figure 5: R_{sign} vs $Re(j)$, $Im(j) = 0.1$, $h = 0$.

Figure 6: $|\langle M \rangle|$ vs $Re(j)$ where $Im(j) = 0.1$, $h = 0$.

Figure 7: Ratio of MC error radii of magnetisation.

Figure 8: $|\langle \chi \rangle|$ vs $Re(j)$ where $Im(j) = 0.1$, $h = 0$.

Figure 9: Ratio of MC error radii of susceptibility.

Figure 10: Improved $|\langle \chi \rangle|$ vs $Re(j)$. Expansion shown as line.

Figure 11: Improved $\langle \chi \rangle$ vs $Re(j)$. Expansion shown as line.

Figure 12: R_{sign} vs $Re(j)$ and linear lattice dimension, $0.1 < Re(j) < 0.3$
 $Im(j) = 0.1$, $h = 0$.

Figure 13: R_{sign} vs $Re(j)$ and linear lattice dimension, $0.5 < Re(j) < 0.8$
 $Im(j) = 0.1$, $h = 0$.

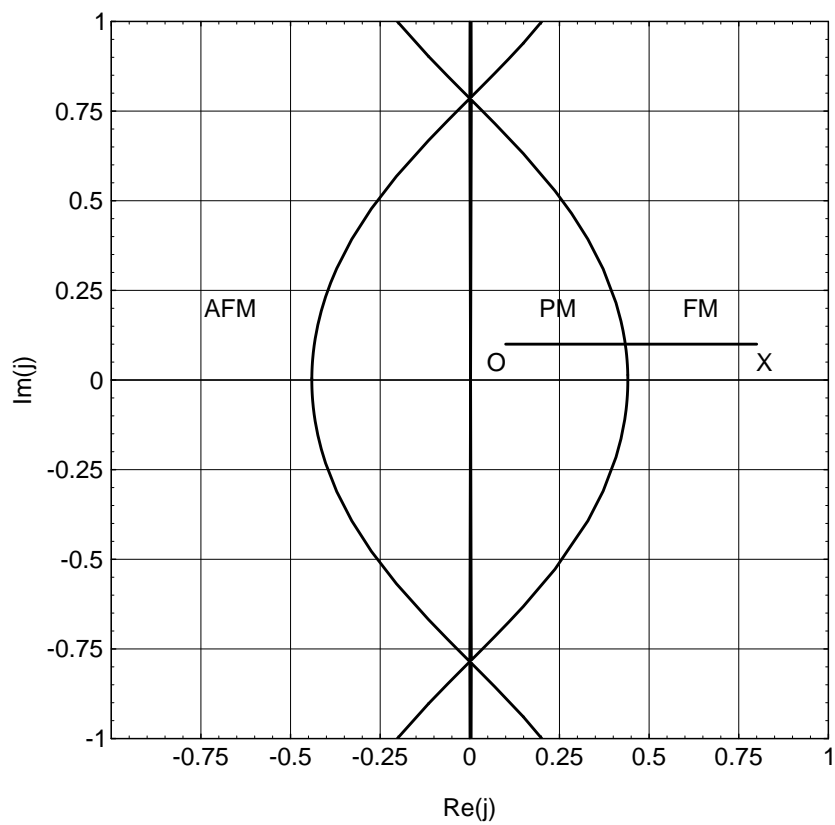


Figure 1

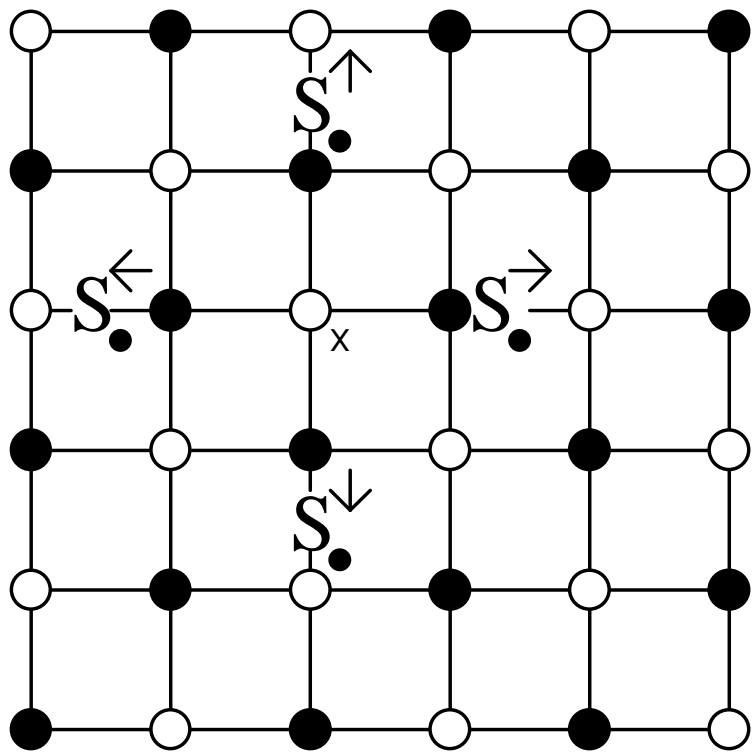


Figure 2

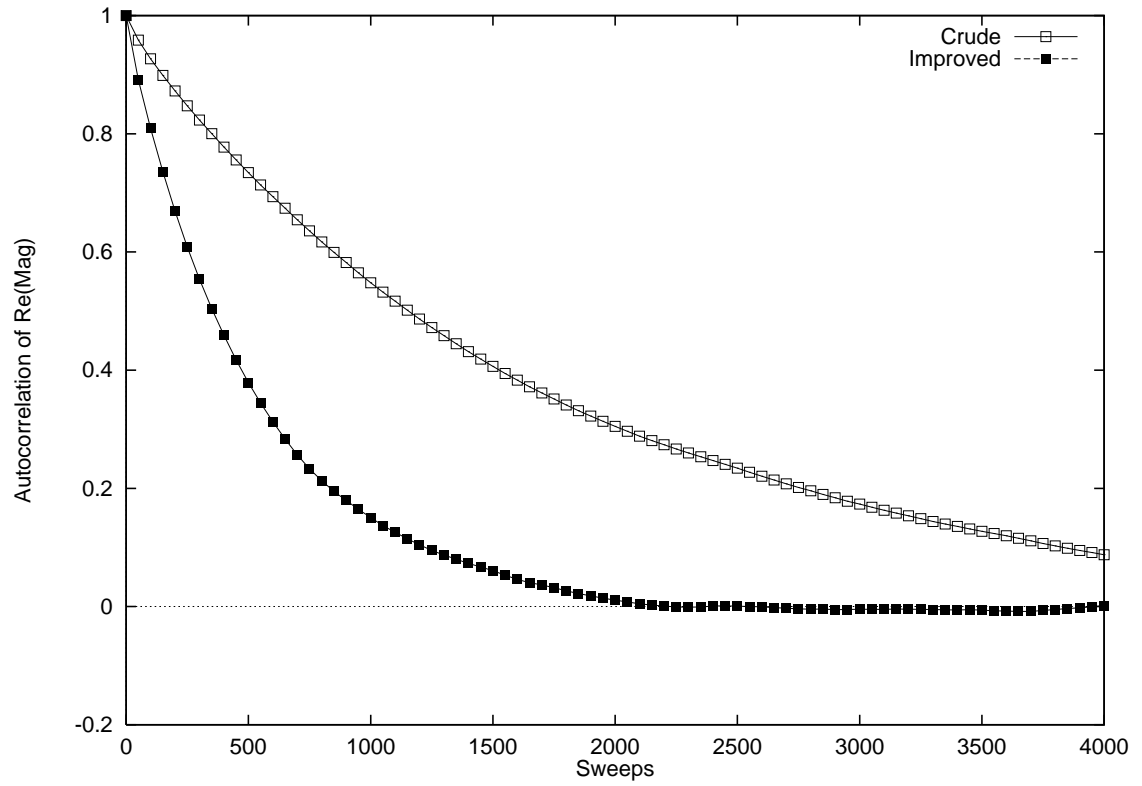


Figure 3

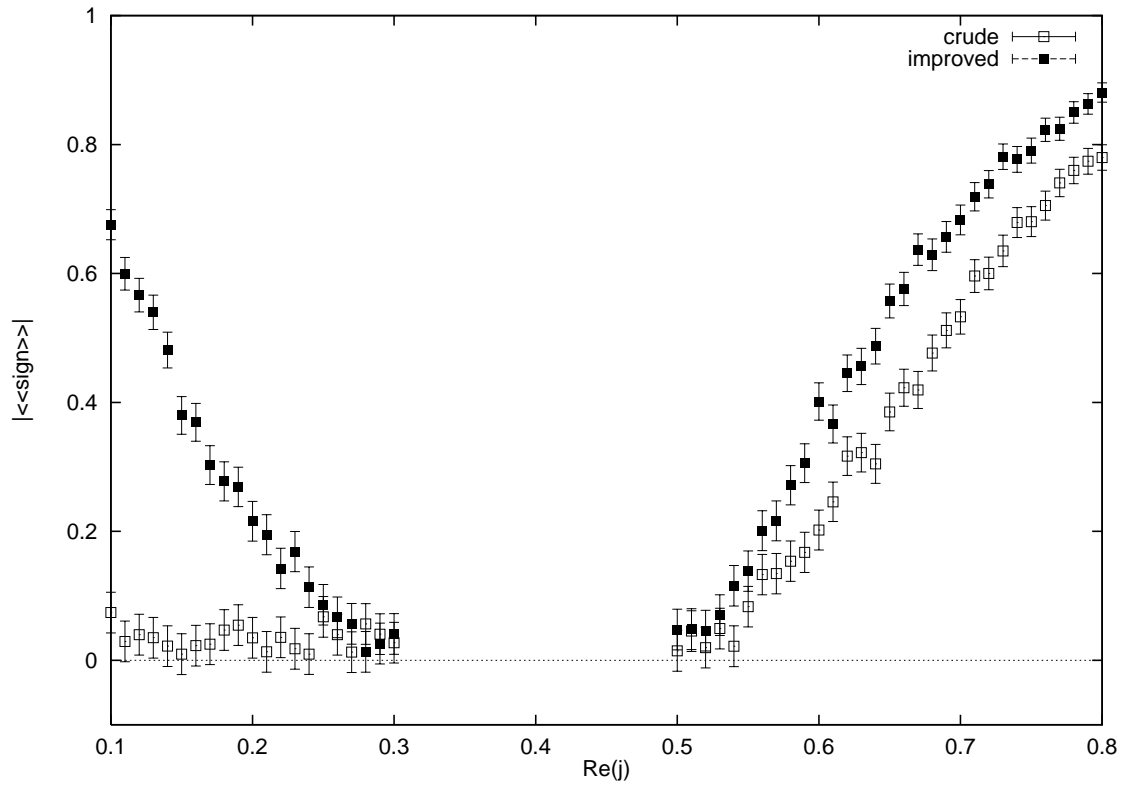


Figure 4

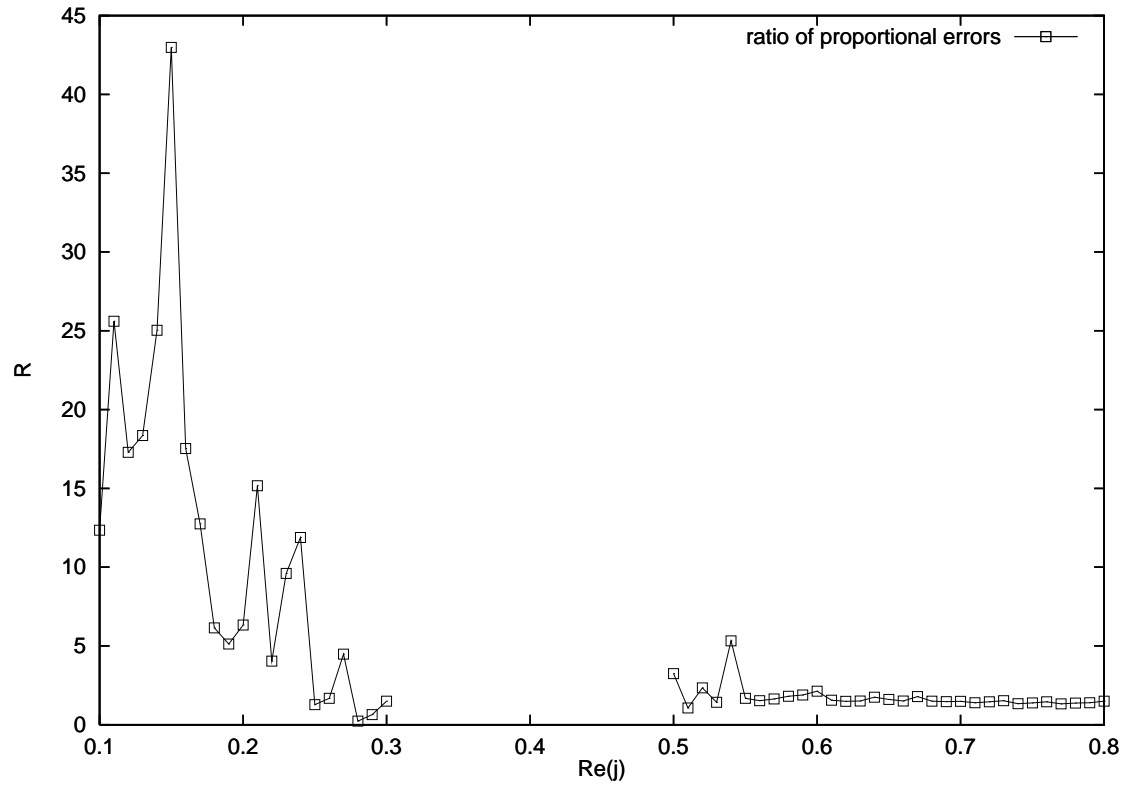


Figure 5

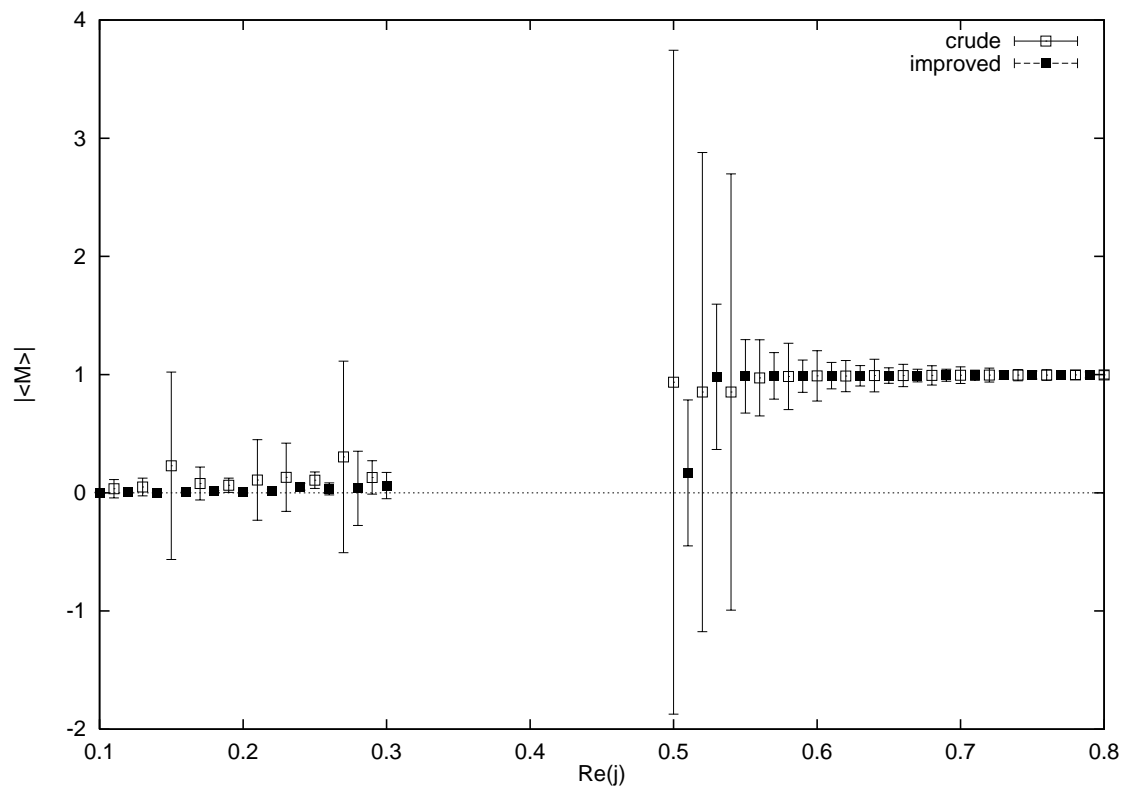


Figure 6

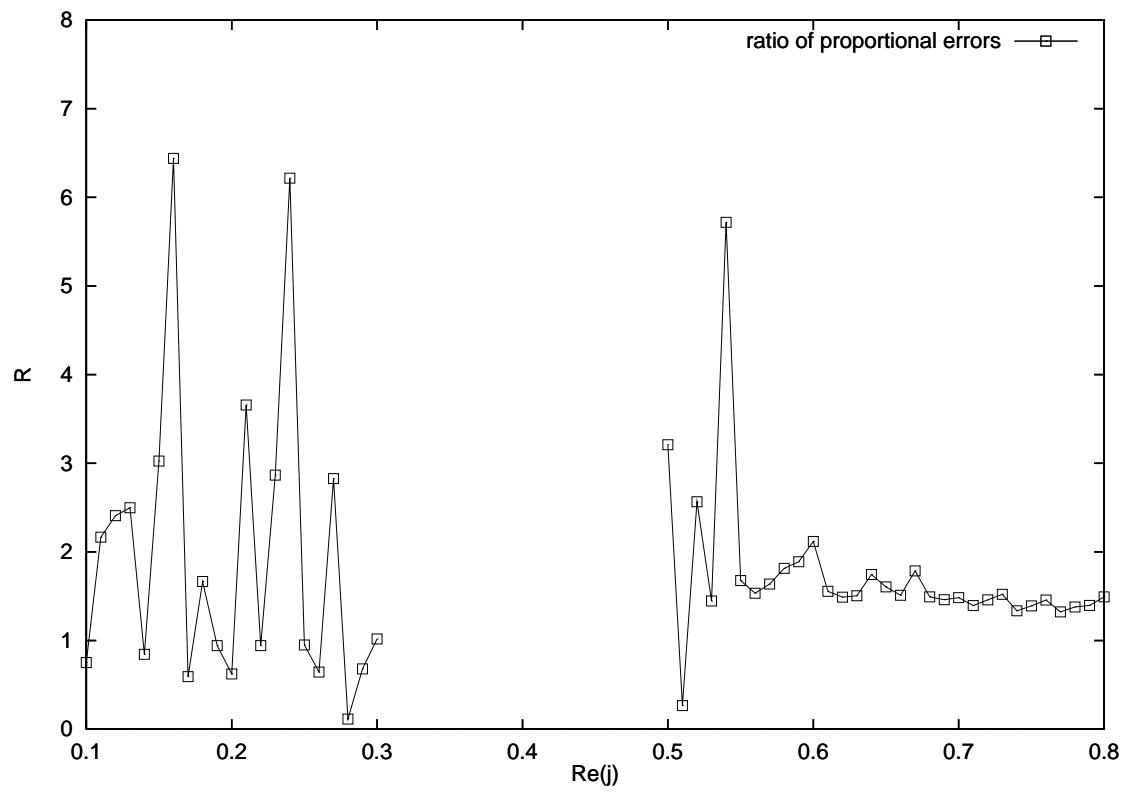


Figure 7

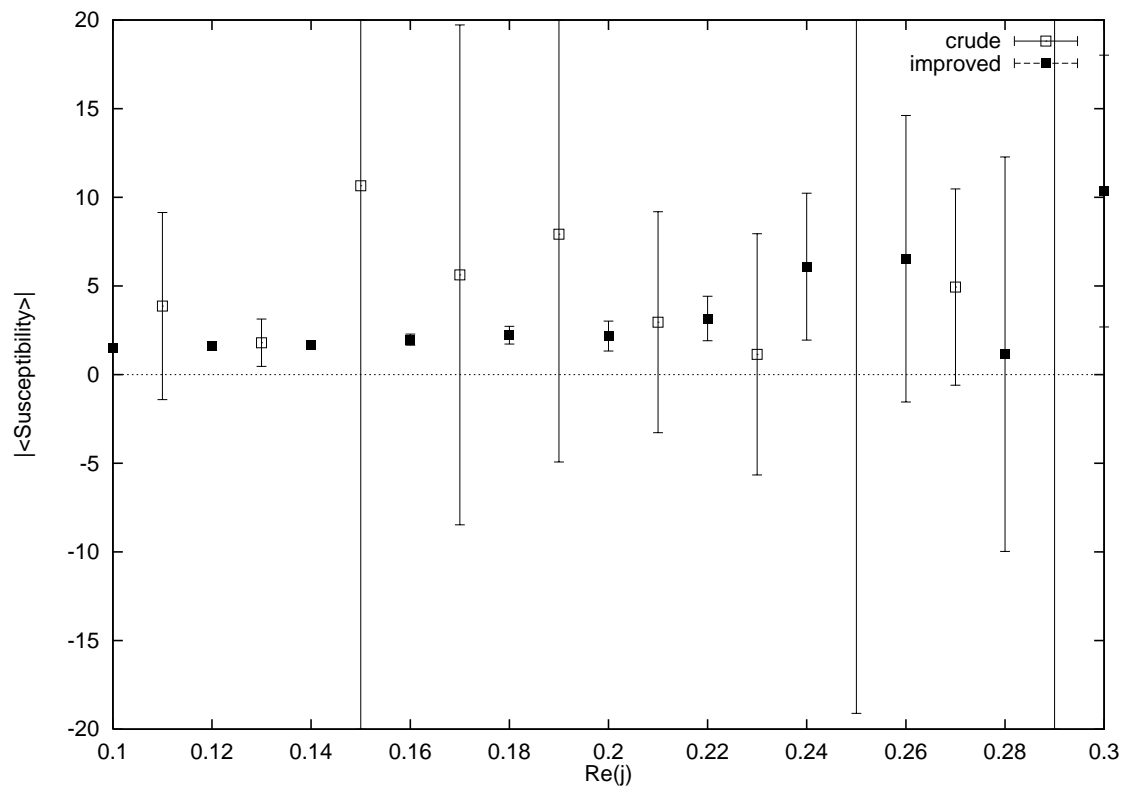


Figure 8

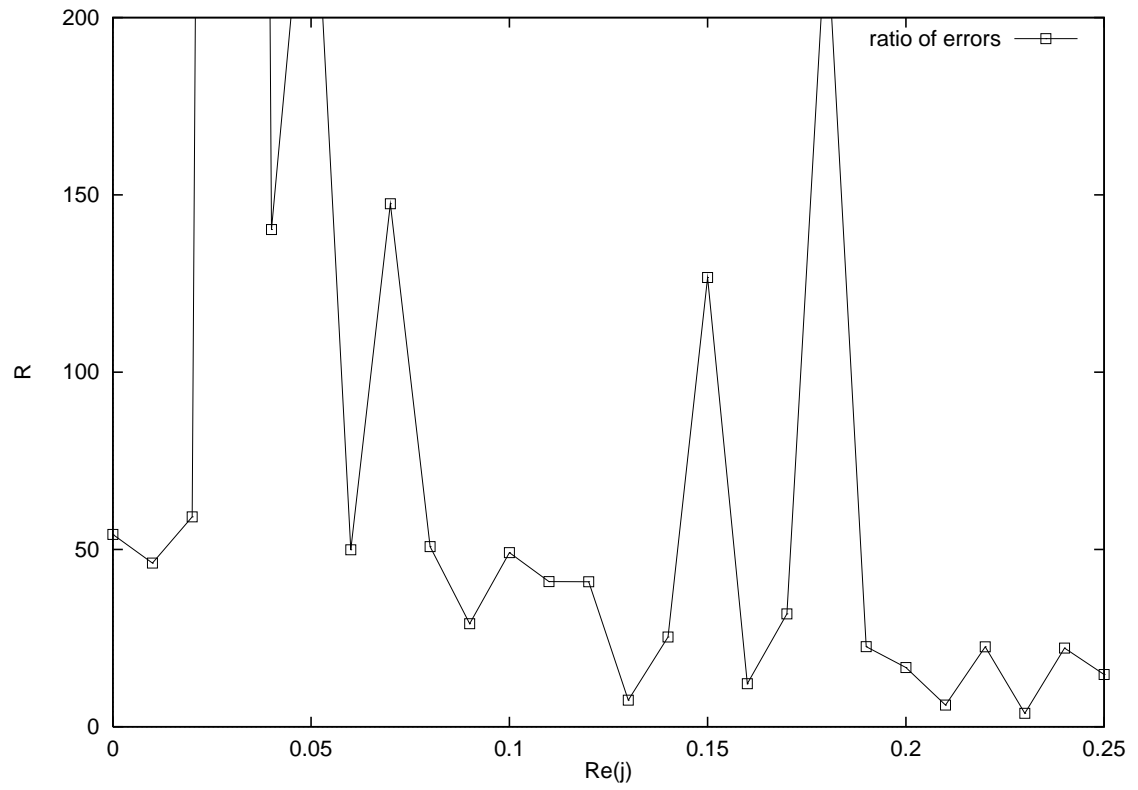


Figure 9

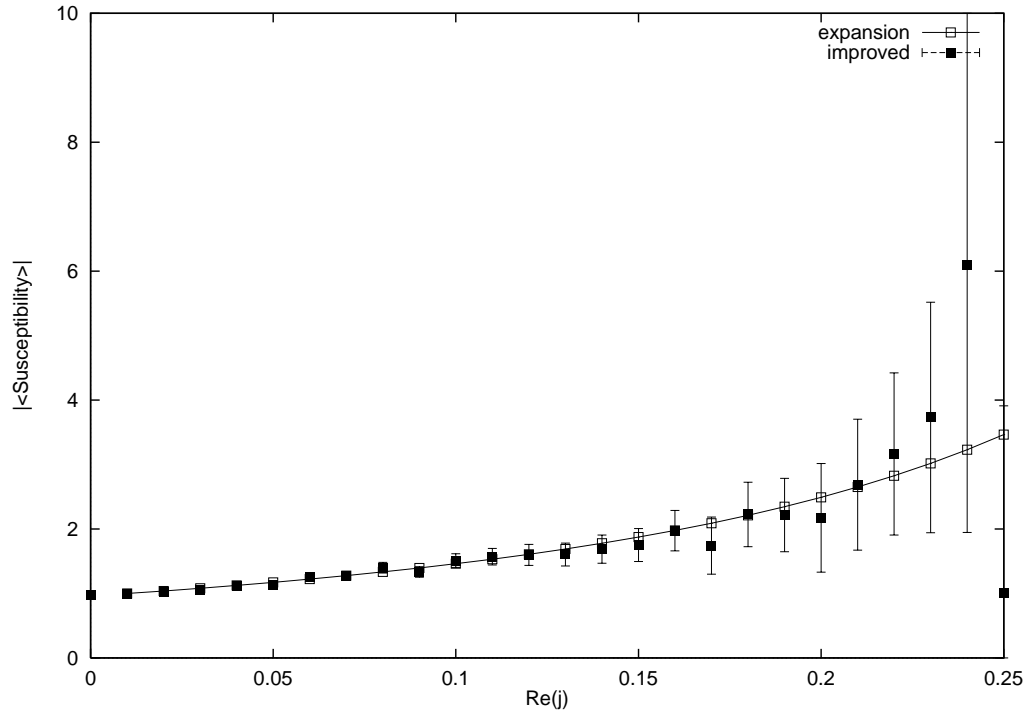


Figure 10

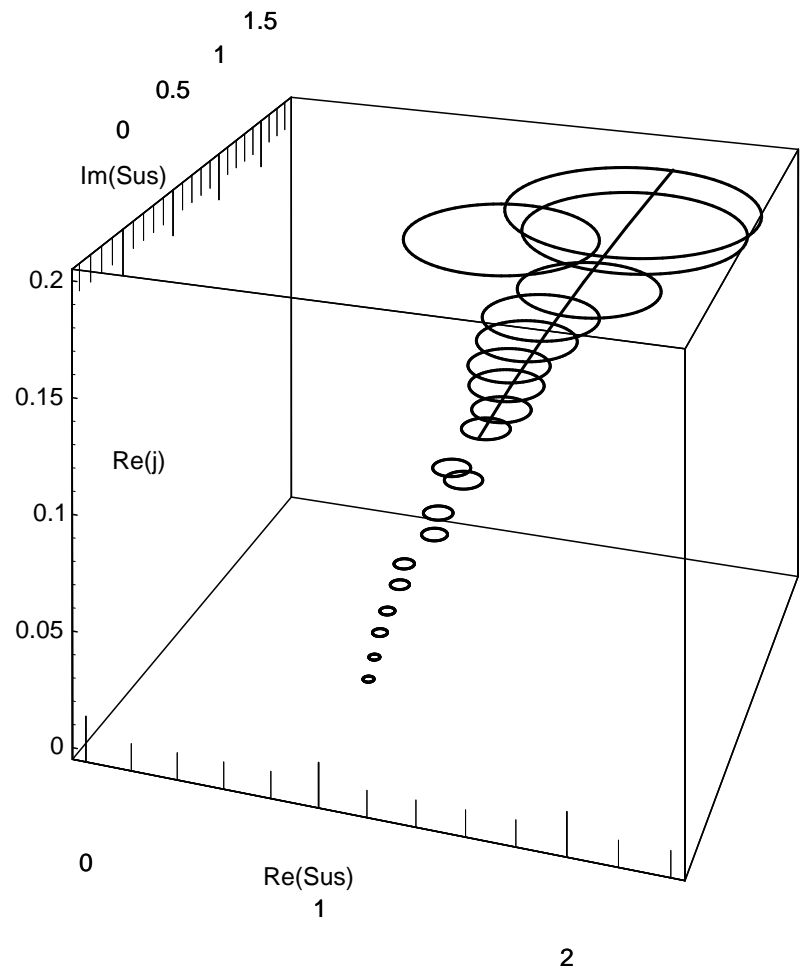


Figure 11

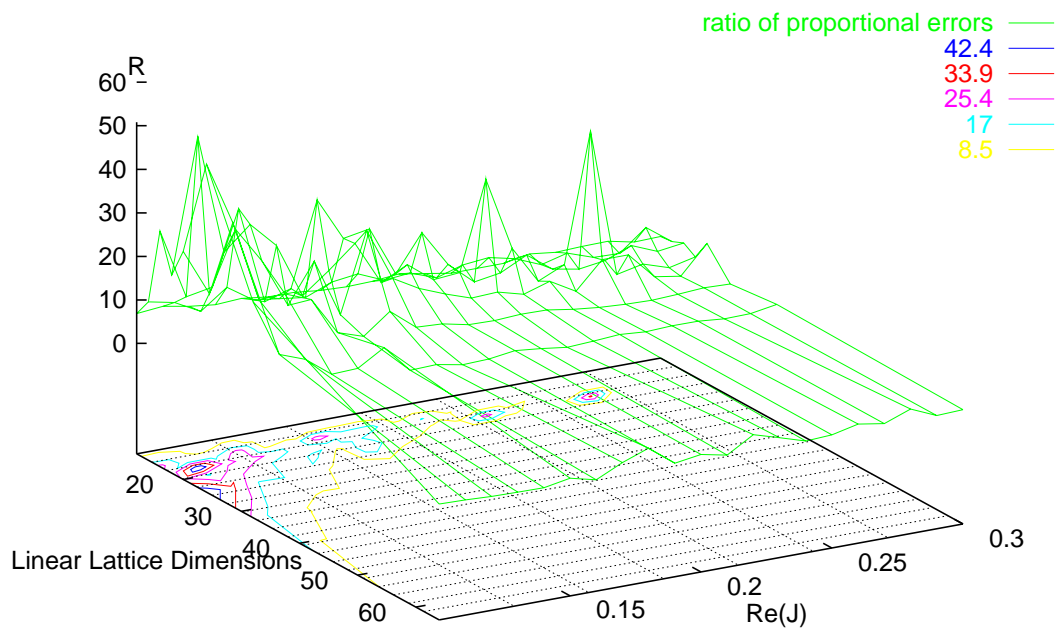


Figure 12

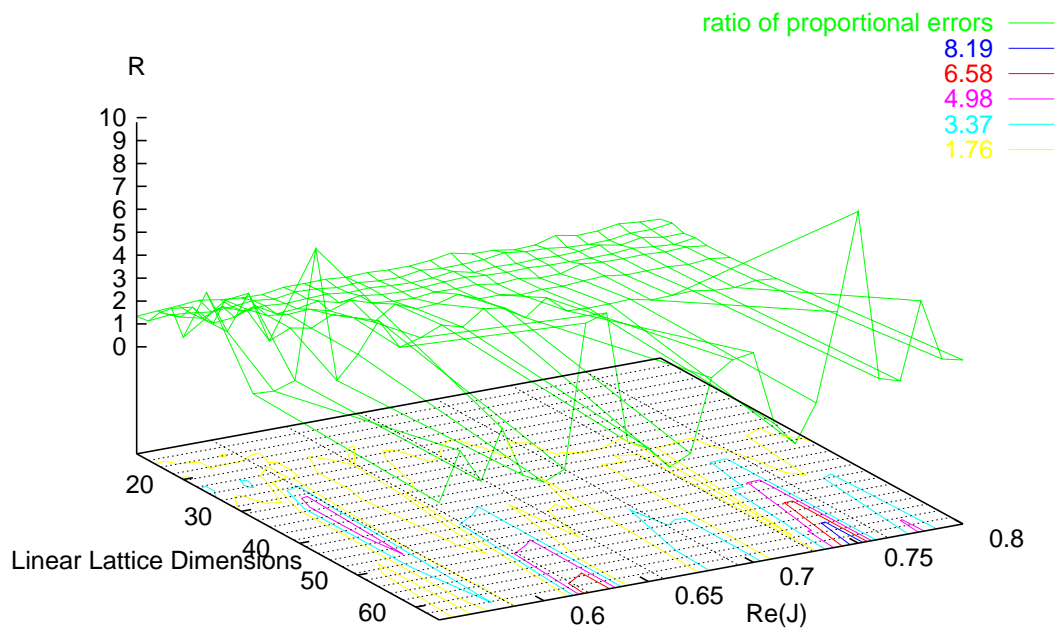


Figure 13